OATAO
Open Archive Toulouse Archive Ouverte

Open Archive Toulouse Archive Ouverte (OATAO)

OATAO is an open access repository that collects the work of Toulouse researchers and makes it freely available over the web where possible

This is an author's version published in: http://oatao.univ-toulouse.fr/21712

Official URL: https://doi.org/10.1109/ICELMACH.2016.7732705

To cite this version:

Ramos chavez, Jose ioav and Diénot, Jean-Marc and Vidal, Paul-Etienne and Viguier, Christophe and Nogarède, Bertrand *Capacitive couplings modeling in concentrated windings.* (2016) In: XXIIth International Conference on Electrical Machines, ICEM'2016, 4 September 2018 - 7 September 2018 (Lausanne, Switzerland).

Any correspondence concerning this service should be sent to the repository administrator: tech-oatao@listes-diff.inp-toulouse.fr

Capacitive couplings modeling in concentrated windings

J. I. Ramos Chávez, J-M. Dienot, P-E. Vidal, C.Viguier, B. Nogarède

***Abstract* -- Parasitic couplings are a major contributor to electromagnetic emissions in conducted and radiated mode in electrical systems. High-frequency behavior is also determined by complex capacitive couplings among others. The faster switching of power converters feeding the machines are a major concern for premature ageing and overvoltages liked to parasitic capacitances. In this work, thorough analytical modeling of parasitic couplings between turns and the core for concentrated winding topologies is presented. The results are compared to numerical simulations.**

***Index Terms*— Electrical Machines, Modeling, EMC, Parasitics**

I. NOMENCLATURE

TABLE I
SYMBOLS AND PARAMETERS

Symbol	Definition
R	Ferromagnetic core radius
l_t	Length of a copper turn
r_0	External radius of an enameled copper wire
r_c	Radius of the copper in an enameled wire
e	Coating thickness of an enameled wire
i	Insulating dielectric film thickness
ε_0	Permittivity of free space
ε_{r_c}	Relative permittivity of the enamel coating
ε_{r_f}	Relative permittivity of the insulating film
ε_{r_R}	Relative permittivity of the resin impregnation

II. INTRODUCTION

MOTORS and generators are very complex electromagnetic structures combining a wide range of materials and architectures. The complex arrangement of the windings into the ferromagnetic yokes of the machine makes it very difficult to parameterize its geometry and calculate parasitic couplings.

The presence of parasitic elements as inductive loops, capacitive couplings and damping through dissipative phenomena in the motor/generator's structure contribute to its low and high frequency (wide band) signature. Besides, they define its Common Mode (CM) and Differential Mode (DM) currents and voltages [1]–[3].

Increasing values of dV/dt and dI/dt and electrical architecture specifications in embedded systems along with severe electromagnetic environments, are to be integrated into the design of motors and generators for mechatronic assemblies. Thus, new and increasing potential perturbations modify the conventional state-of-the-art methods of modeling the entire mechatronic assembly for EMC/EMI purposes, and consequently, the machine itself.

An essential part of the high frequency modeling of the actuator is the modeling of the capacitive couplings created within the motor/generator since these coupling strongly contribute to CM currents [4]–[7].

In this study, the analytical modeling of capacitive couplings in concentrated windings is carried out. First, general hypotheses and considerations are described. Then, analytical modeling of the main couplings found in concentrated windings is developed. Finally, a comparative analysis is done between analytical calculation results and Finite Element Analysis (FEA).

III. GENERAL HYPOTHESES FOR THE ANALYTICAL MODELING

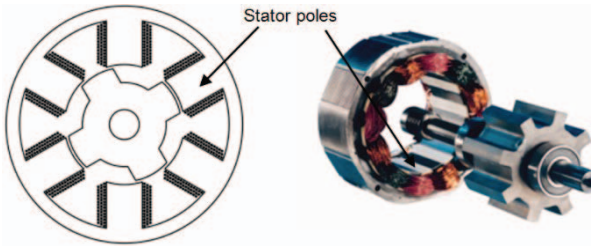

Fig. 1. Concentrated winding design in motors.

Motors with concentrated winding structures usually have rectangular cross-section wound stator poles as described in Fig. 1 [8]. Consequently, the modeling is adapted to such geometries. First, it is assumed that the electric field lines are contained in the planes perpendicular to the copper turns' cross-section and are locally shared between turns and the core. Then, it is considered that turns are not helicoidally but circularly wound over the core. With these hypotheses, a 2-dimensional analysis frame is thus adopted.

In Fig. 2 is schematically shown a portion of a generic concentric winding structure composed of two winding coils around an insulated ferromagnetic core each one isolated from one another by a dielectric film. The turns of both windings are enameled with a thin coating thickness around the copper turn. The axis accounts for the 2D- axisymmetric geometry taken into account for the consolidation of the capacitive coupling models. Dielectric materials are considered to behave linearly with respect to their excitation and, copper

This research work is supported by Novatem SAS, *Advanced Mechatronics*. 3 rue Merlin de Thionville, 11111-FR, Coursan.
Scientific resources have been supported by the EMI/EMC Plat-form LABCEEM, University P. Sabatier, FR-65000 Tarbes (jm.dienot@iut-tarbes.fr).

J. I. Ramos, Dr. Eng. C. Viguier and Pr. Dr. Eng. B. Nogarède work with Novatem SAS, Advanced Mechatronics, Toulouse, FRANCE, 3 rue Merlin de Thionville, 11111-FR, Coursan. (ji.ramosch@novatem-sas.com). B. Nogarède is also with BNCE SAS, holding of Novatem.
Pr. Dr. J-M. Dienot and Dr. Eng. P-E. Vidal are with the Laboratoire Génie de Production at INP-ENIT, Toulouse University, 47 av. d'Azeirex, 65000-FR, Tarbes.

turns and ferromagnetic core are considered to be perfect conductors.
Because of symmetries, electric field lines are considered to be equally shared between adjacent conductors of the inner layers.

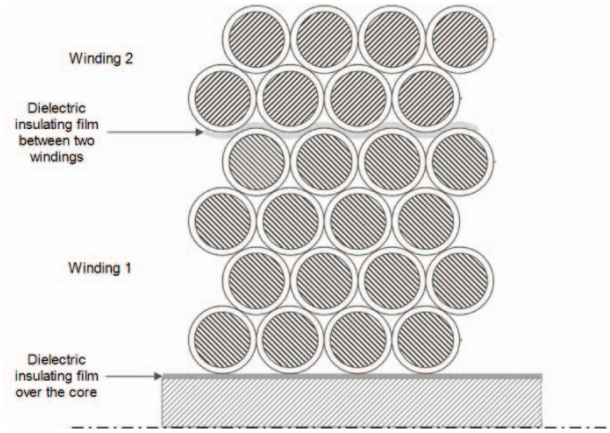

Fig. 2. Cross-sectional view of a portion of concentrated winding.

The study will be divided into 8 elementary cases which should be sufficient to cover a large set of possible configurations with coils with similar characteristics as resumed in Table II.

TABLE II
MODELED CAPACITANCES IN DIFFERENT CONFIGURATIONS

Case	Description	Name
1	Turn-to-turn capacitance without impreg.	C_{tt}
2	Turn-to-core capacitance without impreg.	C_{tc}
3	Turn-to-core through film	C_{tc_f}
4	Turn-to-turn through insulating film	C_{tt_f}
5	Turn-to-turn capacitance with impregnation	$C_{tt_{imp}}$
6	Turn-to-core capacitance with impregnation	$C_{tc_{imp}}$
7	Turn-to-core through film and impregnation	$C_{tc_{f_{imp}}}$
8	Turn-to-turn through film and impregnation	$C_{tf_{f_{imp}}}$

Other specific considerations concerning particular cases will be discussed in the respective section.
The resulting analytical models are then confronted to Finite Element (FE) simulations and measurements on actual windings.

IV. ANALYTICAL MODELING

Fig.3 shows a schematic representation of a cross-section of a portion of a concentric-wound structure. The ferromagnetic core has no insulation over its surface. Only the coating thickness of the turns are ensuring the electrical insulation to the core.
This geometry can be found in certain HF filter coils. Only few turns are represented in the figure for clarity purposes.
In the subsequent sections these elementary couplings are dealt with taking into account the 8 configurations stated above.

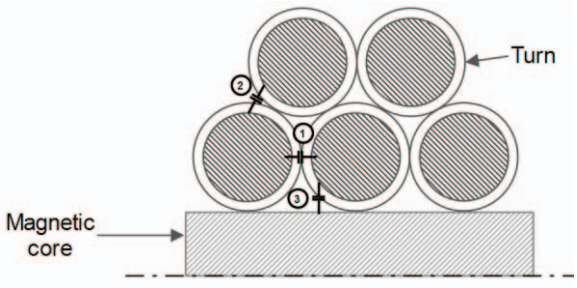

Fig. 3. Representation of capacitive couplings between turns and core.

A. *Case 1: turn-to-turn capacitance*

The turn-to-turn capacitance calculations are inspired on the work presented in [9] and is a continuation of the work developed in [10].
For the inner layers, the calculation of turn-to-turn capacitance can be reduced to the analysis of the ABCD cell representing the assumed electric field lines mean paths between two turns because of symmetries. In fact, for concentric windings, a single turn from a given layer will share its electric field lines with two other turns from the adjacent layer. Due to symmetries in this kind of winding, the assumptions can be extended for the same-layer coupling, considering the turns to be in two different but adjacent layers as in Fig. 4. Besides, for symmetry reasons, all $\vec{E}$ lines are equally shared between adjacent turns. Capacitance for non-adjacent turns is neglected compared to that for adjacent turns.

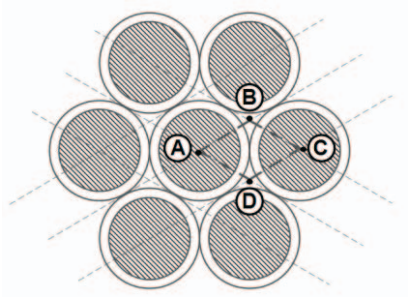

Fig. 4. Coupling mechanism for the inner turns of the winding.

Thus, field lines going from one turn to the other, go through the coating thickness of the first turn, then the airgap formed by the three adjacent turns and finally coating thickness of the second turn.
Since conductor surfaces are considered to be equipotentials, electric field lines are orthogonal to the conductor surfaces. Besides, since the coating thickness e is small to the copper wire radius r_c, lines in the coatings are considered to be orthogonal to the conductor surface as shown in Fig. 5.

Furthermore, because of the proximity effect, electric field lines are concentrated around the shortest distance between two different equipotentials. Thus, $\vec{E}$ lines are considered to be parallel and close to small values of θ. As a first approximation, for the external layer of the winding, it is considered that because of the proximity effect, electric field

lines between turns of the layer are shared in the same way that for the turns of the inner layers. ≤ θ≤ π/6.

This especially means, that no electric field lines travel through greater distances than those mentioned above. And thus, non-adjacent turns have no capacitive coupling whatsoever.

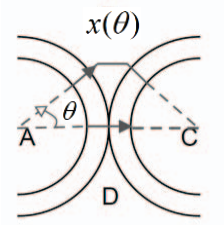

Fig. 5. Assumed path x for field lines between adjacent conductors for –π/6

For the first layer adjacent to the core, the lines between turns are also considered to be shared equally than for the inner layers. The basis of this assumption is again the proximity effect that will make the electric field lines to be concentrated at the closes path between turns.
This is not the case however for the turn-to-core capacitance which is discussed in the latter sections.
In general terms, the elementary capacitance dC between the equivalent elementary surfaces dS of two adjacent conductors along a path x can be described as:

$$dC = \varepsilon_r \varepsilon_0 \frac{dS}{dx} \tag{1}$$

The capacitance along the coating of the first turn C_c can then be calculated:

$$dC_c(\theta) = \varepsilon_{r_c} \varepsilon_0 \frac{r}{dr} d\theta dl \tag{2}$$

By integrating over the turn length, (III.3-19) yields:

$$dC_c(\theta) = \varepsilon_{r_c} \varepsilon_0 \frac{l_t}{ln\left(\frac{r_0}{r_c}\right)} d\theta \tag{3}$$

For the airgap, the capacitance C_g can be calculated considering that in this region

$$x(\theta) = D_0(1 - cos\theta) \tag{4}$$

thus yielding:

$$dC_g(\theta) = \varepsilon_0 \frac{l_t}{2(1 - cos\theta)} d\theta \tag{5}$$

Finally, for the third segment is the same as for the coating of the first turn. Thus, the total turn-to-turn capacitance can be written as **the series combination** of the calculated capacitances:

$$C_{tt} = \frac{C_c\, C_g}{2C_g + C_c} \tag{6}$$

From hypotheses stated in Fig. 5, the integration of the element dθ hast to be taken from $\theta = -\frac{\pi}{6}$ to $\theta = \frac{\pi}{6}$. The resulting total capacitance for this case is given in Table VII.

B. Case 2: Turn-to-core capacitance

Considering the iron core surface as an equipotential, the path taken by the E lines is described as:

$$x(\theta) = r_0(1 - cos\theta) \tag{7}$$

In that case, turn-to-core electric field lines go through half of the path compared to the turn-to-turn case as shown in Fig. 6.

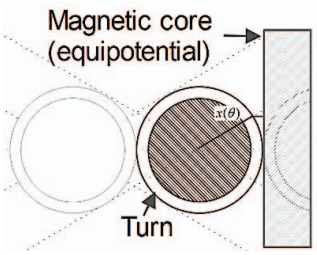

Fig. 6. Assumed path x for the turn-to-core mechanism.

The short distance from the inner turns to the core increases the proximity effect, and thus, the effective exchange surface is considered to be narrowed to an angle aperture of $\theta = -\frac{\pi}{4}$ to $\theta = \frac{\pi}{4}$. The resulting turn-to-core capacitance can be modelled similarly as for the turn-to-turn capacitance for half the path and integrated over $\theta = -\frac{\pi}{4}$ to $\frac{\pi}{4}$ is given in Table VII.

C. Case 3: Turn-to-core capacitance with film

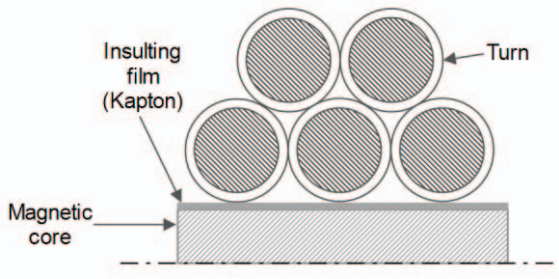

Fig. 7. Structure with an insulated core.

The introduction of a dielectric medium, as in Fig. 7, modifies the above considered path of the electric field lines. These, are not actually orthogonal to the core in the dielectric film region as considered above. But, assuming, that the thickness i of the dielectric film being very small (25-125 µm), the electric field lines can still be considered to be orthogonal to the surface of the core in the dielectric film region as for the $\vec{E}$ lines in the coating thickness of the copper as mentioned before. Therefore, the only difference is that a series capacitance C_f of the film has to be included, yielding:

$$dC_f(\theta) = \frac{\varepsilon_0 \varepsilon_{rf} l_t r_0}{i} cos(\theta)\, d\theta \tag{8}$$

And therefore the resulting capacitance is given in Table VII.

D. Case 4: Turn-to-turn capacitance with film

Fig. 8 shows the structure under analysis and Fig. 9 shows the elementary cell as for Case 1 (c.f. Fig. 4).

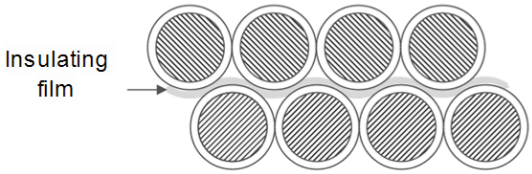

Fig. 8. Two layers separated by an insulating film.

As long as the condition $i \ll r_0$, the distance h can be linked to the dielectric thickness i by the approximation: $h = i * cos(\pi/6)$.

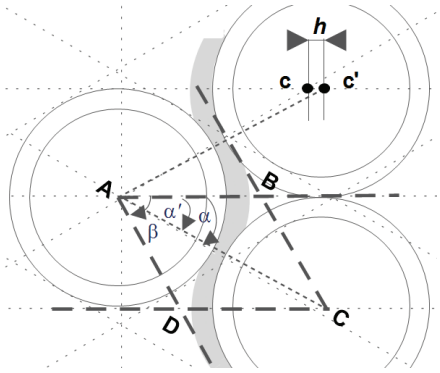

Fig. 9. Elementary cell for turn-to-turn calculation.

The turn-to-turn capacitance calculation can be narrowed to the ABC cell. Since $i \ll r_0$ then $\alpha \approx \alpha'$ and thus, by a rotation of an angle of π rad, the cell ABC is the same as ADC. The capacitance calculated over ABC will have to be doubled.
However, the thickness of the dielectric film is not negligible compared to the coating thickness of the turn. Four segments of the main path depicted in Fig. 10 are identified.

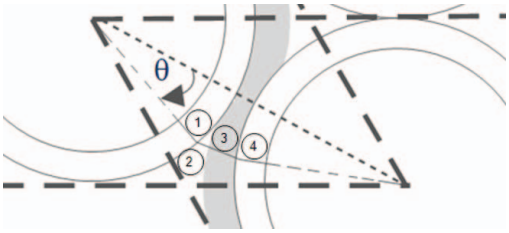

Fig. 10. Four different paths identified.

The path length through the airgap is considered to be small enough compared with the turn radius. $\vec{E}$ lines follow a similar behavior as for the simple turn-to-turn case. $\vec{E}$ lines are considered to be perpendicular to the common tangent to the circle formed by a turn of radius r_0 and a turn including the dielectric film of radius $r_0 + i$ as shown in Fig. 10 (region (2)). From this analysis, it is obvious that, taking the symmetry axis of the turn-to-turn mechanism, the calculations are exactly the same as for the turn-to-core with insulating film case but only over $\theta = -\frac{\pi}{6}$ to $\theta = \frac{\pi}{6}$. Thus, the overall turn-to-turn capacitance with the insulating film **involves double the distance** as in the turn-to-core case. Therefore, the final expression of the turn-to-turn capacitance with an insulating film is obtained by dividing by 2 the value of the turn-to-core capacitance with half the thickness of the insulating film ($i/2$) and integrating only for $\theta = -\frac{\pi}{6}$ to $\theta = \frac{\pi}{6}$. The expression is given in Table VII.

E. Case 5: Turn-to-turn capacitance (impregnated)

For the same difference of voltage potential between two given conductors, the electric field intensity $|\vec{E}|$ is formally ε_r times less important in the presence of a dielectric media than in the vacuum [11]. Therefore, all the partial capacitances of the airgaps calculated here before, see their value increased by a factor equal to the value of the relative permittivity of the dielectric material (epoxide resin in this case) it was replaced with.
In the case of the turn-to-turn mechanism, symmetries force the electric flux lines to be equally shared between turns, so the surface aperture is the same as for the air case even with the presence of the resin impregnation. Thus, the only change in the turn-to-turn capacitance for an impregnated winding is the increase in the partial "airgap" capacitance as follows:

$$dC_g(\theta) = \varepsilon_{r_R}\varepsilon_0 \frac{l_t}{2(1-cos\theta)} d\theta \qquad (9)$$

The overall turn-to-turn capacitance in an impregnated winding is given in Table VII.

F. Case 6: Turn-to-core capacitance (impregnated)

Furthermore, for the turn-to-core mechanism, an increase of the permittivity is equally taken into account. But, apart from that increase in relative permittivity of the airgap, the presence of a dielectric body eases the exchange of electric field lines between the core and the inner turns over a wider surface. So the angle aperture is larger than in the case of air-filled airgap.

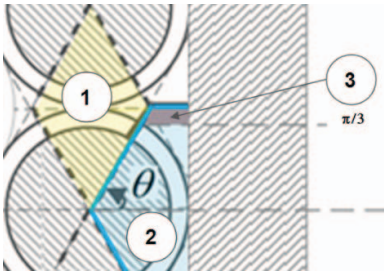

Fig. 11. Discretization area between an inner turn and the bare core.

In Fig. 11 is diagrammed the discretized space available between the inner turns and the core. The discretization takes into account the remaining area left from the aforementioned symmetries for the turn-to-turn couplings ($\theta = \frac{\pi}{3}$ to $\theta = \frac{\pi}{2}$ in this figure) and the symmetries concerning the inner turns and the core (zone 2).To take a bigger surface of exchange into account, the angle aperture will be taken from $\theta = -\frac{\pi}{3}$ to $\theta = \frac{\pi}{3}$ and up to the tangent line between two inner turns (zone 2).

However, taking the expression of the path through the airgap as in eq. (5), a small amount of $\vec{E}$ lines wouldn't be taken into account (zone 3). Although this area would be ignored, the proximity of the turns to the core is still a major factor for the field lines to concentrate close to the core rather than the adjacent turns. So the hypothesis taken here is that all the field lines are concentrated in the clear zone 2 minus both surfaces of zone 3.

The turn-to core mechanism thus becomes (refer to the development of case 2) integrated between $\theta = -\frac{\pi}{3}$ to $\theta = \frac{\pi}{3}$. Turn-to-core capacitance in impregnated windings is resumed in Table VII.

G. *Case 7: Turn-to-core with film and impregnation*

The mechanisms are similar. The turn-to-core capacitance with a dielectric film is expressed as the series combination of the turn-to-core capacitance for an impregnated winding and the partial capacitance yielded by the thin dielectric film (cf. Table VII).

H. *Case 8: Turn-to-turn with film and impregnation*

For the last case scenario processed in this study, the turn-to-turn capacitance for two insulated windings with a dielectric film inserted in between, the modified airgap partial capacitance is included in case 4 will be reused. This final expression is also given in Table VII.

V. FINITE ELEMENT ANALYSIS COMPARISON OF RESULTS

In order to challenge the validity of the models established above, FEA is performed. A two-dimension model such as for the analytical model is built and parameterized to include different materials, coating thickness and insulating layouts.

A. *Hypothesis and setup*

As for the analytical modeling of capacitive couplings, the problem is considered to be axisymmetric. The axis of the circular geometry is considered to be the axis of the magnetic core. The software used for the analysis is Finite Element Method Magnetics (FEMM) [12], a magnetostatic and electrostatic FEA free software for two-dimensional problem solving. The equipotentials (copper turns and core) are set to fixed voltages as follows:

TABLE III
EQUIPOTENTIAL CONDITIONS FOR ENERGY CALCULATIONS

Equipotential	Voltage
High potential	1 V
Low potential	0 V

The output variable for the analysis is the electrostatic energy stored in the segmented areas circumventing the copper turns (dielectric materials or air) and along the surface of the core. The energy calculated in each region yields:

$$Ws = \frac{Cs.(\Delta V)^2}{2} \tag{10}$$

Thus, the partial capacitance in the selected area is given by:

$$Cs = \frac{2.Ws}{(\Delta V)^2} \tag{11}$$

The segmentation is made according to the hypothesis stated in the analytical modeling part. As for the turn-to-turn mechanism, it is thus assumed that the couplings outside the segmented areas is negligible compared to the energy stored inside these areas. In Fig. 13 is presented a segmented problem solution in which the field lines (arrows) are mainly concentrated into the segmented areas.

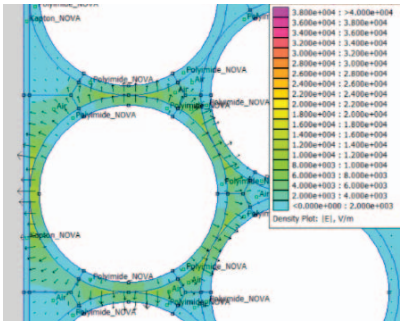

Fig. 13. Segmentation and field lines contained in the specified regions for energy calculation.

B. *Commonly used materials in industrial applications*

In order to compare the analytical and FEA model computation results, a set of different IEC 60317 commonly used Class F-wires were chosen and resumed in Table IV. Only a few set of materials were chosen for the analysis (cf. Table V).

TABLE IV
IEC 60317 CLASS F WIRE SPECIFICATIONS USED IN THE ANALYSIS

Copper diameter	Grade 1 diameter (average)	Grade 2 diameter (average)
mm	mm	mm
0.200	0.220	0.233
0.250	0.274	0.289
0.315	0.342	0.359
0.400	0.430	0.449
0.500	0.534	0.556
0.630	0.668	0.692
0.710	0.750	0.776
0.800	0.843	0.870
1.000	1.048	1.079
1.250	1.301	1.333
1.600	1.654	1.689
2.000	2.057	2.094

TABLE V
MATERIALS PROPERTIES USED IN THE ANALYSIS

Function	Commercial name	Material	ε_r
Core insulation	Kapton®	Polyamide-imide	3.4 (1 kHz)
Wire coating		Polyamide-imide	3.5 (1 MHz)
Impregnation*	AralditeF® Aradur C121/HY905 mix:	Epoxide Resin	3.7 (50 Hz)

C. *Comparative analysis of results and discussion*

In Fig. 14 and Fig. 15, the relative errors between analytical models and FEA models of turn-to-turn cases are presented both for grade and grade wires. Globally, the relative errors are inferior to 30% except for case 7. The general trends are in the sense of error reduction with increasing wire diameter. In

fact, the larger the diameter, the better the hypotheses are respected giving better predictions. A singularity in this general behavior is found with non-impregnated turn-to-turn capacitance when a dielectric film is present as can be seen in Fig. 14 and 15.

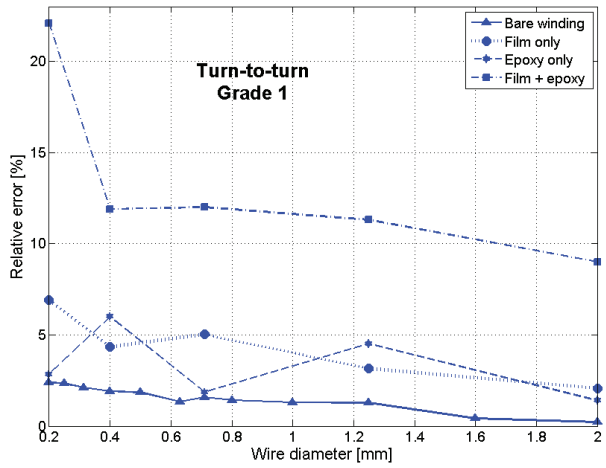

Fig. 14. Comparison of results for turn-to-turn capacitance for Grade 1.

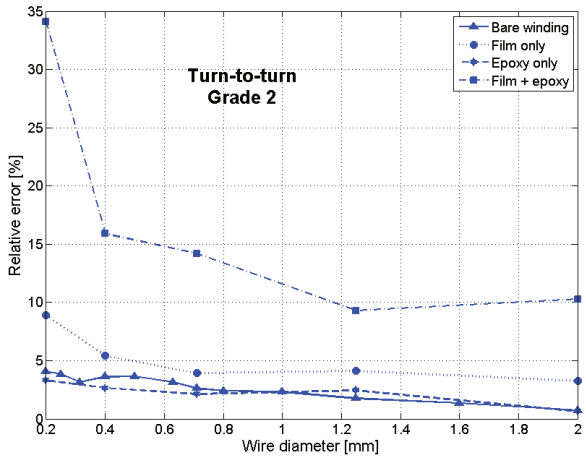

Fig. 15. Comparison of results for turn-to-turn capacitance for Grade 2.

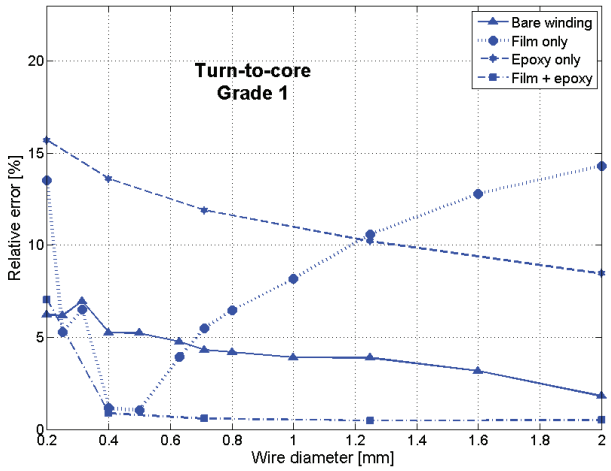

Fig. 16. Comparison of results for turn-to-core capacitance for Grade 1.

Adding a thickness of dielectric materials seems to have a larger impact on the hypotheses of closeness of equipotentials than expected. Then, in Fig. 16 and Fig. 17 the same comparison is made for turn-to-core cases. Finally, concerning the turn-to-core mechanism for the different film thickness, the average relative errors for grade 1 and 2 wire cases are resumed in Table VI.

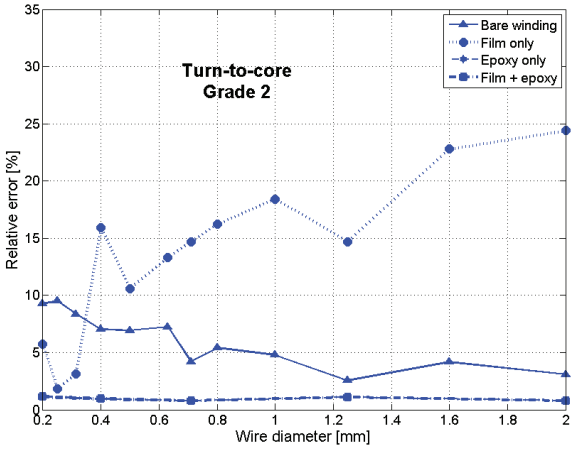

Fig. 17. Comparison of results for turn-to-core capacitance for Grade 2.

The same conclusion is drawn for grade 1 vs. grade 2 insulations since results for grade 1, which is a thiner coating insulation than grade 2 are better overall, compared to FEA results.

TABLE VI
TURN-TO-CORE CAPACITANCE FOR DIFFERENT FILM THICKNESS

	Non-impregnated		Impregnated	
Film thickness	**Grade 1 Avg error**	**Grade 2 Avg error**	**Grade 1 Avg error**	**Grade 2 Avg error**
50 µm	7.44 %	13.5 %	1.9 %	1 %
100 µm	9.44 %	16.3 %	12.3 %	12.5 %
200 µm	20.2 %	23.7 %	32.5 %	29.7 %

The thicker the insulating film, the bigger the difference between analytical and FEA results. This is especially accentuated by the fact that the model doesn't perform well when an insulating film is included. However, for most of the cases, especially for bare windings, errors are very small. Besides, the analytical models, even at 30 % error, are useful to estimate the capacitive behavior with very simple formulations.

VI. CONCLUSIONS

The analytical models here presented were confronted against numerical simulations with acceptable results. Different configurations are available to account for the various concentrated windings layouts. This model lacks of results for materials with very different relative permittivity values but allows to roughly estimate the parasitic capacitances present in concentrated windings with impregnations and other insulating materials. Finally, an experimental validation should be helpful in determining the validity of the above analytical models.

TABLE VII
SUMMARY OF MODELED CAPACITANCES CASE BY CASE

Case reference	Coupling mechanism	Analytical value of the capacitance for a given turn length
Case 1	Turn-to-turn	$C_{tt} = \frac{\varepsilon_0 l_t}{2}\int_{-\pi/6}^{\pi/6} \frac{1}{1+\frac{1}{\varepsilon_{r_c}} ln\left(\frac{r_0}{r_c}\right) - cos\theta} d\theta$
Case 2	Turn-to-core	$C_{tc} = \varepsilon_0 l_t \int_{-\pi/4}^{\pi/4} \frac{1}{1+\frac{1}{\varepsilon_{r_c}} ln\left(\frac{r_0}{r_c}\right) - cos\theta} d\theta$
Case 3	Turn-to-core through insulating dielectric film	$C_{tc_f} = \varepsilon_0.\varepsilon_{rf}.l_t.r_0 \int_{-\pi/4}^{\pi/4} \frac{1}{\left(1+\frac{1}{\varepsilon_{r_c}} ln\left(\frac{r_0}{r_c}\right) - cos\theta\right).\varepsilon_{rf}.r_0.cos\theta + i} d\theta$
Case 4	Turn-to-turn through insulating dielectric film	$C_{tt_f} = \frac{\varepsilon_0.\varepsilon_{rf}.l_t.r_0}{2} \int_{-\pi/6}^{\pi/6} \frac{1}{\left(1+\frac{1}{\varepsilon_{r_c}} ln\left(\frac{r_0}{r_c}\right) - cos\theta\right).\varepsilon_{rf}.r_0.cos\theta + i} d\theta$
Case 5	Impregnated turn-to-turn	$C_{tt_{imp}} = \frac{\varepsilon_0.\varepsilon_{r_R}.\varepsilon_{r_c}.l_t}{2} \int_{-\pi/6}^{\pi/6} \frac{1}{\varepsilon_{r_R}.ln\left(\frac{r_0}{r_c}\right) + \varepsilon_{r_c}.(1-cos\theta)} d\theta$
Case 6	Impregnated turn-to-core	$C_{tc_{imp}} = \varepsilon_0.\varepsilon_{r_R}.\varepsilon_{r_c}.l_t \int_{-\pi/3}^{\pi/3} \frac{1}{\varepsilon_{r_R}.ln\left(\frac{r_0}{r_c}\right) + \varepsilon_{r_c}.(1-cos\theta)} d\theta$
Case 7	Impregnated turn-to-core through insulating dielectric film	$C_{tc_{f_{imp}}} = \varepsilon_0.\varepsilon_{r_R}.\varepsilon_{r_f}.\varepsilon_{r_c}.l_t \int_{-\pi/3}^{\pi/3} \frac{cos\,\theta}{\varepsilon_{r_f}.cos\theta\left(\varepsilon_{r_R}.ln\left(\frac{r_0}{r_c}\right) + \varepsilon_{r_c}.(1-cos\theta)\right) + \frac{i}{r_0}\varepsilon_{r_R}\varepsilon_{r_c}} d\theta$
Case 8	Impregnated turn-to-turn through insulating dielectric film	$C_{tt_{f_{imp}}} = \frac{\varepsilon_0.\varepsilon_{r_R}.\varepsilon_{r_f}.\varepsilon_{r_c}.l_t}{2} \int_{-\pi/6}^{\pi/6} \frac{cos\,\theta}{\varepsilon_{r_f}.cos\theta\left(\varepsilon_{r_R}.ln\left(\frac{r_0}{r_c}\right) + \varepsilon_{r_c}.(1-cos\theta)\right) + \frac{i}{2.r_0}\varepsilon_{r_R}\varepsilon_{r_c}} d\theta$

VII. REFERENCES

[1] E. Zhong, T. Lipo, and others, "Improvements in EMC performance of inverter-fed motor drives," *Ind. Appl. IEEE Trans. On*, vol. 31, no. 6, pp. 1247–1256, 1995.

[2] S.-P. Weber, E. Hoene, S. Guttowski, W. John, and H. Reichl, "Modeling induction machines for EMC-Analysis," in *Power Electronics Specialists Conference, 2004. PESC 04. 2004 IEEE 35th Annual*, 2004, vol. 1, pp. 94–98 Vol.1.

[3] M. Schinkel, S. Weber, S. Guttowski, W. John, and H. Reichl, "Efficient HF modeling and model parameterization of induction machines for time and frequency domain simulations," in *Applied Power Electronics Conference and Exposition, 2006. APEC'06. Twenty-First Annual IEEE*, 2006, p. 6–pp.

[4] U. R. G Grandi, "High-Frequency Behavior of Three-Phase Induction Motor Windings," Electrimotion Conference, Bologne, Italy, 2001.

[5] R. G. Rhudy, E. L. Owen, and D. K. Sharma, "Voltage Distribution Among the Coils and Turns of a Form Wound AC Rotating Machine Exposed to Impulse Voltage," *IEEE Power Eng. Rev.*, vol. PER-6, no. 6, pp. 40–41, Jun. 1986.

[6] V. Mihaila, "Nouvelle conception des bobinages statoriques des machines à courant alternatif pour réduire les effets négatifs des dv/dt,", Artois, PhD. Thesis 2011.

[7] G. Skibinski, R. Kerkman, D. Leggate, J. Pankau, and D. Schlegel, "Reflected wave modeling techniques for PWM AC motor drives," in *Applied Power Electronics Conference and Exposition, 1998. APEC '98. Conference Proceedings 1998., Thirteenth Annual*, 1998, vol. 2, pp. 1021–1029 vol.2.

[8] B. Nogarède and D. V. den Bossche, *Electrodynamique appliquée : Fondements et principes physiques de l'électrotechnique Cours et exercices corrigés*. Paris: Dunod, 2005.

[9] A. Massarini and M. K. Kazimierczuk, "Self-capacitance of inductors," *IEEE Trans. Power Electron.*, vol. 12, no. 4, pp. 671–676, Jul. 1997.

[10] J. I. Ramos, J.-M. Dienot, P.-E. Vidal, C. Viguier, and B. Nogarède, "Contribution to modeling of parasitic couplings for predicting EMC behavior of electrical machines," in *2014 International Conference on Electrical Machines (ICEM)*, 2014, pp. 1056–1062.

[11] *Electrodynamics of Continuous Media, Second Edition: Volume 8*, 2 edition. Butterworth-Heinemann, 1984.

[12] "Finite Element Method Magnetics," 07-Jan-2016. [Online]. Available: http://www.femm.info/wiki/HomePage. [Accessed: 07-Jan-2016].

VIII. BIOGRAPHIES

José Ioav Ramos Chavez was born in Mexico City in 1988 and obtained his Electrical Engineering diploma in 2012 from the Institut National Polytechnique of Toulouse (INPT), France. He currently is a third year Ph.D. student at INPT sponsored by NOVATEM and in collaboration with Laboratoire Génie de Production (LGP) and LABCEEM platform in Tarbes, France. His work concerns the study of EMC and wide-band behavior of mechatronic systems and electrical systems in general.

Jean-Marc Dienot received PhD degrees in Microwave Circuits and Applied Electromagnetic, from the University Paul Sabatier, Toulouse, France. He is currently a University Professor in the Institute of Technology, Tarbes, France. Since 1995, he has been involved new EMI/EMC problematic in Electronics' architectures. He has developed and leads the LABCEEM platform, dedicated for research and high-level trainings projects in EMI and EMC domains. He is recipient of scientific certifications and committee's member in domains as Power Electronics, EMC, Instrumentation and Communications.

Paul-Etienne Vidal obtained a Ph.D. degree from INPT in 2004. From 2004 to 2006, he was engaged in electrical machine controls and systems at the laboratory LEEI, INP/Centre National de la Recherche Scientifique (CNRS). Since 2006 he s an associate professor at LGP –INPT. His research topic deals with power converter efficiency, electro-thermo mechanical modeling and simulations.

Christophe Viguier was born in Castres, France, in 1978. He received the M.S. degree in Automation, Electronics and Electrical Engineering from the University Paul Sabatier of Toulouse, France, in 2001. He received PhD degree in EE from the INPT in 2005. He is currently R&D Engineer at NOVATEM which carries development projects of embedded innovative equipment in electrical engineering.

Bertrand Nogarède was born in Montpellier, France, in 1964. He received the Engineering degree in electrical engineering from the ENSEEIHT, Toulouse, France, in 1987 and the Ph.D. degree from the INPT in 1990. He is a University Professor at INPT. He is currently the Scientific and Technical coordinator at BNCE and NOVATEM. Author of *Electrodynamique Appliquée (Dunod, 2005)*, he has worked on modeling and design of electrical innovative machines. Among his various awards, he is laureate of the 2007 Blondel Medal.